ACS APPLIED MATERIALS & INTERFACES

Research Article

www.acsami.org

Designed Fabrication and Characterization of Three-Dimensionally Ordered Arrays of Core–Shell Magnetic Mesoporous Carbon Microspheres

Kaiping Yuan,[†] Renchao Che,*[,†] Qi Cao,[†] Zhenkun Sun,[†] Qin Yue,[†] and Yonghui Deng*[,†]

[†]Laboratory of Advanced Materials, Department of Chemistry and Shanghai Key Laboratory of Molecular Catalysis and Innovative Materials, State Key Laboratory of Molecular Engineering of Polymers, Department of Materials Sciences, Collaborative Innovation Center of Chemistry for Energy Materials, Fudan University, Shanghai 200433, P. R. China

Supporting Information

ABSTRACT: A confined interface coassembly coating strategy based on three-dimensional (3-D) ordered macroporous silica as the nanoreactor was demonstrated for the designed fabrication of novel 3-D ordered arrays of core–shell microspheres consisting of Fe_3O_4 cores and ordered mesoporous carbon shells. The obtained 3-D ordered arrays of Fe_3O_4@mesoporous carbon materials possess two sets of periodic structures at both mesoscale and submicrometer scale, high surface area of 326 m^2/g, and large mesopore size of 19 nm. Microwave absorption test reveals that the obtained materials have excellent microwave absorption performances with maximum reflection loss of up to −57 dB at 8 GHz, and large absorption bandwidth (7.3–13.7 GHz, < −10 dB), due to the combination of the large magnetic loss from iron oxides, the strong dielectric loss from carbonaceous shell, and the strong reflection and scattering of electromagnetic waves of the ordered structures of the mesopores and 3-D arrays of core–shell microspheres.

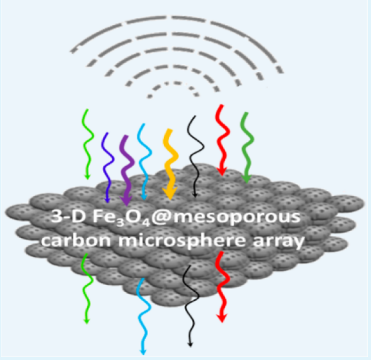

KEYWORDS: *interface coassembly, mesoporous carbon, magnetic nanomaterials, core–shell structures, microwave absorption*

INTRODUCTION

Magnetic nanomaterials, due to their outstanding properties such as paramagnetism, magnetic separability,[1−3] and Neel relaxation effect,[4] have captivated tremendous research interests for applications in various fields, including magnetic resonance imaging (MRI),[5] bioseparation[6−8] catalysis,[9] energy storage,[10] and microwave absorption.[11] Particularly as a typical microwave absorber, magnetite (Fe_3O_4) nanoparticles have gained much attention due to their significant advantages in microwave absorption, such as the strong absorption characteristics, wide absorption frequency range, and low cost.[12,13] Magnetite nanoparticles with diversified morphologies, including the nanodendrites,[14] nanorods,[15] two-dimensional nanolamellar and microspheres,[16] have been extensively studied to reveal the dependency of microwave performance on the morphology. Dendrite-like Fe_3O_4 nanoparticles synthesized via hydrothemal reactions have been proved to possess a good microwave absorption performance in the low and middle frequency range (2–9 GHz).[14] Wang et al.[17] adopted a templating synthesis method for Fe_3O_4 nanolamellars that exhibit a strong microwave absorption with a reflection loss of −46.6 dB at 3 GHz.

According to the basic principle of microwave absorption, the loss mechanism of microwave absorber consists of magnetic loss and dielectric loss.[18−20] Magnetite as the microwave absorber mainly contributes the magnetic loss due to its intrinsic magnetic property. Therefore, to develop high-performance microwave absorbers with both magnetic loss and dielectric loss, many fabrication strategies have been explored to combine magnetite nanomaterials with other nanomaterials that can contribute remarkable dielectric loss and electromagnetic impedance balance. To date, various multicomponent Fe_3O_4-based nanomaterials have been investigated.[21−23] In this regard, owing to their strong dielectric loss, metal oxides[24] and carbon nanomaterials such as carbon nanotubes (CNTs),[25] reduced graphene oxide (*r*GO),[26] and carbon nanocoils[27] have been widely used as complementary components for Fe_3O_4 as microwave absorbers. On the other hand, ordered mesoporous materials, due to their regular arrays of mesopores that are tunable pore sizes of 2–50 nm, have recently been demonstrated to possess excellent performance as microwave absorbers.[28−31] Guo et al.[32] synthesized sandwich-like magnetic mesoporous silica microspheres by coating iron oxide particles successively with nonporous silica and mesoporous silica. Compared to the parent iron oxides, the obtained composites displayed improved microwave absorption performance with stronger absorption characteristics and broader absorption frequency range, which is due to the strong reflection and scattering of electromagnetic waves in the pore

Received: December 9, 2014
Accepted: February 3, 2015
Published: February 3, 2015

DOI: 10.1021/am508683p
ACS Appl. Mater. Interfaces 2015, 7, 5312−5319

Scheme 1. Synthetic Route for the 3-D Ordered Arrays of Fe_3O_4@*meso*Carbon Microspheres with Core−Shell Structure through the Confined Interface Coating Strategy

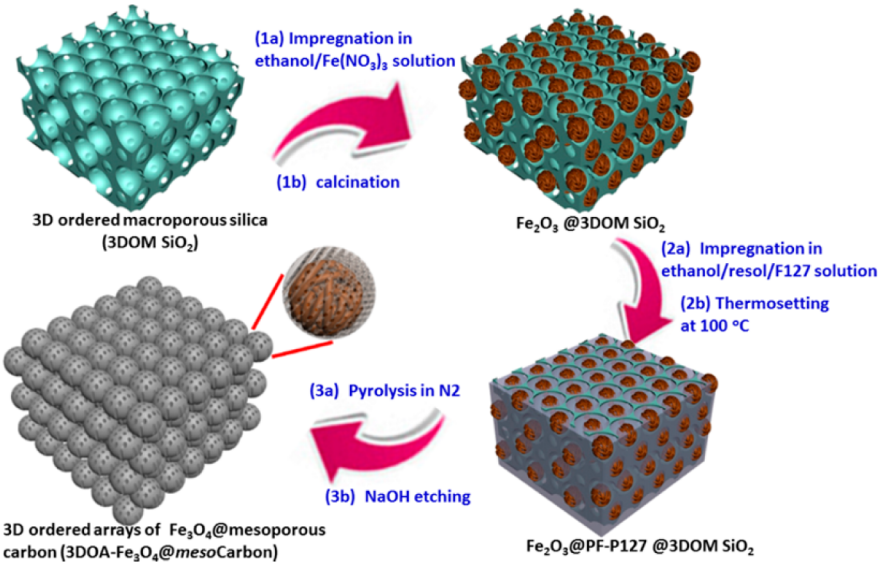

channels of mesoporous silica and their multilayered core−shell structure.

Wiley and co-workers reported that ordered arrays of magnetic microspheres exhibit unique magnetic phenomena, including angle-dependent magnetization, due to their ordered structures.[33] In light of this finding, it could be expected that the microwave absorption performance of Fe_3O_4-based multicomponent nanomaterials with well-aligned structures may possess unique microwave absorption enhancement. So far, much effort has been devoted to synthesizing magnetic nanomaterials-based microwave absorbers; however, most of these nanomaterials were utilized in the form of nanocomposites with ill-defined structures, and little work has been done to study the microwave absorption behaviors of the periodically arranged magnetic nanocomposites, especially carbon-coated magnetite microspheres with well-defined core−shell structure.

Herein, we report a confined interface coating strategy for the fabrication of novel three-dimensionally ordered arrays of core−shell microspheres consisting of Fe_3O_4 cores and ordered mesoporous carbon shells. Three-dimensionally ordered macroporous silicas (3DOM-SiO_2) were employed as the nanoreactor for deposition of single iron oxide particle with controlled size in each macropore and further coating iron oxide particle individually with a layer of mesoporous carbon. The subsequent removal of 3DOM-SiO_2 template leads to three-dimensional (3-D) arrays of mesoporous carbon-coated magnetite particles (denoted as 3DOA-Fe_3O_4@*meso*Carbon) monolith with high surface area of 326 m^2/g and large pore size of 19 nm. The obtained 3DOA-Fe_3O_4@*meso*Carbon materials exhibit excellent microwave absorption performance with maximum reflection loss of up to −57 dB at 8 GHz and large absorption bandwidth (7.3−13.7 GHz and <−10 dB). Such an excellent performance is mainly attributed to the combination of individual merit of each component and the ordered nanostructure, that is, the large magnetic loss from iron oxides, the strong dielectric loss from carbonaceous shell, as well as the strong reflection and scattering of electromagnetic waves of the ordered structures of microsphere arrays and mesopore channels.

EXPERIMENTAL SECTION

Chemicals. The Pluronic block copolymer poly(ethylene oxide)-*b*-poly(propylene oxide)-*b*-poly(ethylene oxide) (F127, M_w = 12 600, $EO_{106}PO_{70}EO_{106}$) was purchased from Aldrich Corporation. Phenol (AR), tetraethyl orthosilicate (TEOS, AR), absolute ethanol (AR), hydrochloric acid (AR), ferric nitrate ($Fe(NO_3)_3·9H_2O$, AR), sodium hydroxide (NaOH, AR) were purchased from Shanghai Chemical Reagent Corporation. All chemicals were used as received without further purification, and in all experiments, purified water (Millipore) with the resistivity larger than 18 MΩ·cm was utilized. Resol, a soluble phenolic resin with relatively low molecular weight of ∼500 g/mol, was first prepared according to previous report[34] and dissolved in ethanol to form a solution with the resol concentration of 20 wt %.

Fabrication of Three-Dimensionally Ordered Macroporous Silicas. For the fabrication of 3DOM-SiO_2, monodispersed polystyrene (PS) microspheres with different sizes (900−1200 nm) were synthesized via a soap-free emulsion polymerization process.[35,36] After washing with ethanol and water three times, the purified PS spheres were redispersed in ethanol and allowed to form sedimentation for a week under gravity to form colloidal crystals. Afterward, the supernatant ethanol was removed carefully, and the obtained colloidal crystals were dried at 35 °C for 10 h and further annealed at 100 °C for 1 h. Thus, the monolithic PS colloidal crystals were prepared for further use. A typical procedure for making 3DOM-SiO_2 is described as follows. An ethanol solution of TEOS precursor (2.08 g of TEOS, 0.3 g of H_2O, 0.9 mL of 2 M HCl, and 15 g of ethanol) was drop-casted on several pieces of the colloidal crystals (1 cm × 1 cm × 1 cm) made of 1200 nm PS microspheres. After evaporation of ethanol at 30 °C for 24 h, the composite monolith was scratched carefully with a blade to remove the excess gel precursors. Finally, the impregnated colloidal crystals were calcined in air at 550 °C for 6 h using 1 °C/min of ramping rate to remove PS microspheres, and thus the 1200 nm-3DOM-SiO_2 monolith was obtained.

For the synthesis of Fe_2O_3@3DOM-SiO_2 monoliths with a porous Fe_2O_3 particle filled inside each macropore, the obtained 1200 nm-3DOM-SiO_2 monolith was impregnated in the $Fe(NO_3)_3$ ethanol solution (4.04 g of $Fe(NO_3)_3$ dissolved in 10 mL of absolute ethanol) for 3 h at 30 °C for evaporation of ethanol in 6 h. This impregnation process was repeated three times. At last, the excess gel precursor of the composite monolith was scraped off carefully, and the obtained composites were finally calcined in air at 550 °C for 4 h to obtain the 1200 nm-Fe_2O_3@3DOM-SiO_2 sample.

Templated Fabrication of Three-Dimensional Ordered Arrays of Microspheres with Core−Shell Structure. For the

DOI: 10.1021/am508683p
ACS Appl. Mater. Interfaces 2015, 7, 5312−5319

synthesis of 3DOA-Fe_3O_4@Carbon microspheres, small pieces (~0.5 g) of 1200 nm-Fe_2O_3@3DOM-SiO_2 monoliths were placed in a Petri dish, and then a clear precursor solution containing resol (5.0 g) and ethanol (15 g) was dropwise added into the petri dish. Time was allowed for a complete evaporation of ethanol completely at 25 °C in 8 h. The process was repeated five times to ensure a complete filling of these spheres. The as-obtained sample was then heated in an oven at 80 °C for 24 h for thermosetting resol into phenolic formaldehyde (PF) resin. The obtained Fe_2O_3-PF@3DOM-SiO_2 composite was afterward carbonized at 500 °C for 3 h under N_2 atmosphere with the ramping rate of 5 °C/min. Finally, the obtained composite was treated in NaOH aqueous solution (5 M) at 80 °C to remove silica, followed with thorough washing with water and ethanol six times, and thus the 1200 nm-3DOA-Fe_3O_4@Carbon sample was prepared.

The 1200 nm-3DOA-Fe_3O_4@*meso*Carbon sample was fabricated via the similar procedure except that the precursor solution containing of resol (5.0 g), ethanol (15 mL), and F127 (2.5 g) was utilized instead. For the fabrication of 800 nm-3DOA-Fe_3O_4@Carbon and 800 nm-3DOA-Fe_3O_4@*meso*Carbon, the synthesis procedures are the same as those for 1200 nm-3DOA-Fe_3O_4@Carbon and 1200 nm-3DOA-Fe_3O_4@*meso*Carbon, except that 800 nm-3DOM-SiO_2 derived from colloidal crystal of 900 nm PS microspheres was used as the template.

Measurements and Characterization. Transmission electron microscope (TEM) characterization was carried out on a JEOL 2100F field-emission TEM (Japan) operating at 200 kV of the working voltage. Scanning electron microscope (SEM) characterization was conducted on a Hitachi S-4800 field-emission SEM (Japan). Also, wide-angle X-ray diffraction (XRD) patterns were recorded on a Bruker D8 Advance powder X-ray diffractometer (Germany) with Ni-filtered Cu Kα radiation (40 kV, 40 mA, 1.5406 Å). Nitrogen adsorption−desorption isotherms were measured at 77 K with a Micromeritics Tristar 3020 analyzer (USA). The samples were previously degassed under vacuum at 180 °C for at least 6 h before measurements, and the specific surface areas were calculated using the Brunauer−Emmett−Teller (BET) method. The pore volumes and distributions of pore sizes were calculated correspondingly utilizing the Broekoff−de Boer sphere model from the adsorption branches of the isotherms. Besides, the total pore volumes (V) were evaluated according to absorbed amounts at 0.995 of the relative pressure (P/P_0).

RESULTS AND DISCUSSION

Scheme 1 illustrates the synthesis protocol for 3DOA-Fe_3O_4@*meso*Carbon based on the confined interface coating process. In the first step, 3DOM-SiO_2 monolith synthesized by replicating 3-D ordered colloidal crystal of polystyrene (PS) microspheres was impregnated in the ethanol solution of $Fe(NO_3)_3$, and then the iron precursor was in situ converted into Fe_2O_3 particles in the macropores via calcination in air, resulting in a unique 3DOM-SiO_2 with each macropore filled with one Fe_2O_3 microsphere (denoted as Fe_2O_3@3DOM-SiO_2). Second, the obtained Fe_2O_3@3DOM-SiO_2 was further impregnated in a precursor solution (a typical precursor for synthesizing ordered mesoporous carbon) containing resol, ethanol, and amphilic block copolymer F127. After evaporation of ethanol, a layer of the resol/F127 composite was formed on the surface of Fe_2O_3 particles, which was converted into PF/F127 composite with ordered mesostructure upon thermosetting treatment at 100 °C. Third, the obtained Fe_2O_3-PF/F127@3DOM-SiO_2 composite was further pyrolyzed in N_2, which causes the carbonization of PF, decomposition of F127, the reduction of Fe_2O_3, and the formation of Fe_3O_4@mesoporous carbon@3DOM-SiO_2. After slowly etching the silica framework by soaking in NaOH solutions, 3-D ordered arrays of Fe_3O_4@mesoporous carbon microspheres (i.e., 3DOA-Fe_3O_4@*meso*-Carbon) were obtained.

Monodisperse PS microspheres with a diameter of 1400 nm were synthesized via a dispersion polymerization method available in previous reports[35,36] and were used to construct 3-D ordered colloidal crystals through the gravimetric sedimentation (Figure 1). With the obtained colloidal crystals

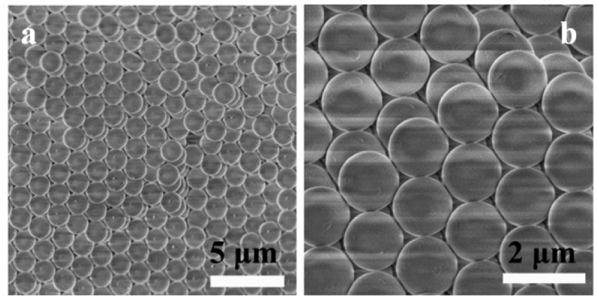

Figure 1. SEM images (a, b) of the highly ordered arrays viewed along [100] directions of the face-centered cubic structured colloidal crystals of 1400 nm PS microspheres.

as templates, silica precursor can be filled in the interstitial voids among the closely packed PS microspheres by impregnation in a siliceous solution. After removing PS microspheres via calcination, 3DOM-SiO_2 monolith with intense opalescence and uniform macropores of ~1200 nm was obtained (Figure 2a and inset). The macropore size is a

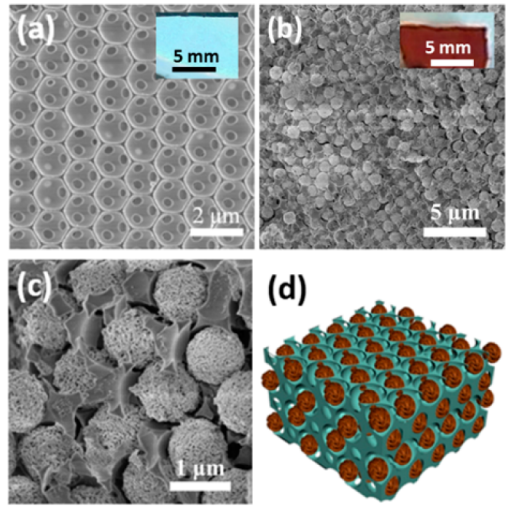

Figure 2. SEM images of (a) the 3-D ordered macroporous SiO_2 (3DOM-SiO_2) and (b, c) Fe_2O_3@3DOM-SiO_2 obtained after deposition of Fe_2O_3 particle in the macropore. (d) The structure model of Fe_2O_3@3DOM-SiO_2. (insets) The photographs of the correponding monolithic samples.

little smaller than the diameter of PS microspheres due to the shrinkage of silica framework during calcination at high temperature. As measured from the scanning electronic microscopy (SEM) image, 3DOM-SiO_2 has a large macropore window of ~200 nm, which greatly facilitates the diffusion of liquid solutions during impregnation and thus favors the introduction of guest precursors into the macropores.

Notably, with the facile hard templating synthesis method, 3DOM-SiO_2 with different macropore diameter and connecting window size can be readily fabricated using PS microspheres of different sizes. For example, by using colloidal crystals of 900 nm PS microspheres as the template, 3DOM-SiO_2 with

DOI: 10.1021/am508683p
ACS Appl. Mater. Interfaces 2015, 7, 5312−5319

macropores of 800 nm and window size of 100 nm can be obtained (Supporting Information, Figure S1a,b). The uniform and well-connected macropore of 3DOM-SiO_2 is an ideal "nanofactory" for the confinement fabrication of ordered arrays of uniform guest nanomaterials. In this study, iron oxide precursor was introduced into the macropores by repeated impregnation of 3DOM-SiO_2 in $Fe(NO_3)_3$/ethanol solutions, followed with evaporation of ethanol. After calcination at 450 °C in air, brown Fe_2O_3@3DOM-SiO_2 monolithic materials were obtained (Figure 2b, inset). Clearly, in the scanning electronic microscopy (SEM) image, the macropores were individually filled with iron oxide microspheres, which form ordered arrays throughout the entire 3DOM-SiO_2 monolith (Figure 2b). The iron oxide microspheres have diameter of ~900 nm, which is smaller than the macropore size (1200 nm) due to the significant volume shrinkage during conversion of iron precursor into iron oxides, and interestingly, the iron oxide microspheres exhibit porous structure (Figure 2c). The generation of porous iron oxides in this confined synthesis is probably due to the unique solid-phase conversion of iron precursor confined in the macropores that possess numerous nucleation sites in the curved surface of 3DOM-SiO_2 monolith for the growth of iron oxide. Besides, the release of NO_2 during the calcination treatment can also contribute to the formation of disordered nanopores.

Since the porous Fe_2O_3 particles are smaller than the macropores, the voids between iron oxide microspheres and silica framework is accessible for deposition of mesostructured resol-F127 composites through impregnation of Fe_2O_3@3DOM-SiO_2 composites in the precursor solution. Thus, after thermosetting and pyrolysis treatment, the iron oxide microspheres can be in situ coated by a layer of mesoporous carbon in the macropores of 3DOM-SiO_2; meanwhile, iron oxides can be converted into magnetite (Fe_3O_4) by carbon species. The successful formation of mesoporous carbon on the iron oxides is mainly attributed to two factors. First, both the porous iron oxide and 3DOM-SiO_2 are hydrophilic, which is favorable for the impregnation of ethanolic precursor solution. Second, the resol molecules possess lots of phenolic hydroxyl groups, which can interact with both iron oxides through chelating with iron species[34] and F127 via hydrogen binding.[37] Furthermore, the resol/F127/ethanol precursor solution can invade all the remaining space of the macropores in the Fe_2O_3@3DOM-SiO_2 composites, resulting in a complete encapsulation of the porous Fe_2O_3 particle and stable "sintering" of Fe_2O_3@PF-F127 microspheres located in the adjacent macropores due to the thermal polymerization of glue-like resol molecules. After carbonization treatment, Fe_3O_4@*meso*Carbon core–shell microspheres binding with each other were left in the macropores (Figure 3a). Further removal of the silica framework in NaOH solutions leads to 3DOA-Fe_3O_4@*meso*Carbon monolith (Figure 3b). To gain detailed structural information, the monolithic composites were slightly ground for electron microscopy observation. As shown in the SEM image (Figure 3b), the obtained Fe_3O_4@*meso*Carbon microspheres have a uniform diameter of ~1200 nm (denoted as 1200 nm-Fe_3O_4@*meso*Carbon), and they retain the ordered arrays of the 3DOM-SiO_2, indicating a faithful replication process. High-magnification SEM image reveals the presence of irregular stubbles with a diameter of ~150 nm in the surface of microspheres (Figure 3c). Such stubbles are originated from the mechanical cleavage of sintering points (boxed area in Figure 3a) that correlate with connecting windows of the macropores (Figure 3b, inset). The

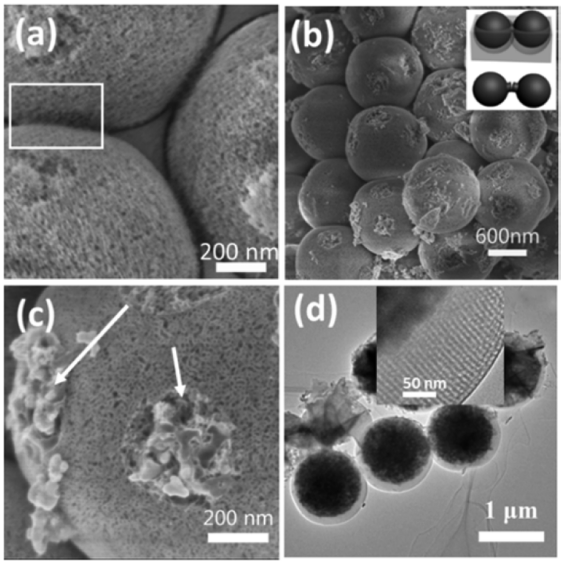

Figure 3. SEM (a–c) and TEM (d) images of the obtained 3DOA-Fe_3O_4@mesoCarbon materials comprising 1200 nm Fe_3O_4@mesoCarbon microspheres with different magnifications.

TEM observation clearly indicates that the obtained Fe_3O_4@*meso*Carbon microspheres have a mesoporous carbon shell of 120 nm in thickness (Figure 3d), and ordered pore channels with a mean diameter of ~18 nm can be clearly seen in the shell (Figure 3d, inset).

Scanning TEM (STEM) observation further reveals a typical core–shell structure of the obtained Fe_3O_4@*meso*Carbon microspheres (Figure 4a). The energy-dispersive X-ray

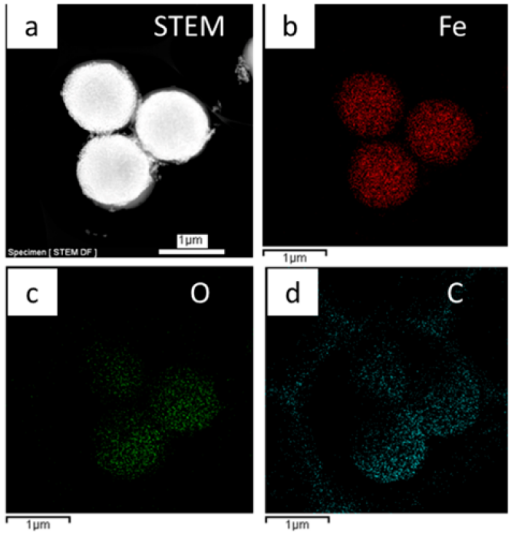

Figure 4. (a) Scanning TEM (STEM) image of 1200 nm 3DOA-Fe_3O_4@mesoCarbon core–shell microsphere and (b–d) the EDX elemental maps of Fe, O, and C, respectively.

(EDX) element mapping results (Figure 4c,d) indicate the presence of Fe, O, and C elements, and the diameter of C-mapped spheres in Figure 4d is much larger than those of Fe- and O-mapped spheres (Figure 4b,c), confirming the presence of iron oxide core and carbon shell. X-ray diffraction (XRD) patterns of the as-made Fe_2O_3@3DOM-SiO_2 composites display well-resolved characteristic diffraction peaks that can

DOI: 10.1021/am508683p
ACS Appl. Mater. Interfaces 2015, 7, 5312–5319

be indexed to the hematite phase with a rhombohedral structure (Figure 5a). The XRD patterns of 1200 nm 3DOA-

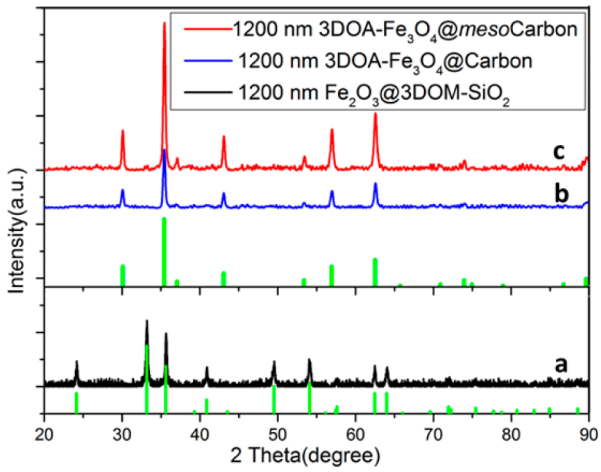

Figure 5. XRD patterns of (a)1200 nm-Fe_2O_3@3DOM-SiO_2, (b) 1200 nm-3DOA-Fe_3O_4@*meso*Carbon, and (c) 1200 nm-3DOA-Fe_3O_4@Carbon. The green patterns correspond to the standard XRD diffraction peaks of α-Fe_2O_3 (lower) and Fe_3O_4 (upper), respectively.

Fe_3O_4@*meso*Carbon microspheres reveal typical diffraction peaks assigned to magnetite (Figure 5b,c), which reflects a phase transformation of α-Fe_2O_3 into Fe_3O_4 in the composites during pyrolysis.

The N_2 absorption−desorption isotherms of the 1200 nm-3DOA-Fe_3O_4@*meso*Carbon sample (Figure 6A) show a type IV curve with a sharp capillary condensation step in the P/P_0 range of 0.8−0.9, which implies uniform and large mesopores. The BET surface area was calculated to be 293 m^2/g. The pore size distribution derived from the adsorption branch using the Barrett−Joyner−Halenda (BJH) method reveals a pore size of 19.2 nm (Figure 6A, inset), much larger than the pore size (~6 nm) of FDU-16. It is mainly due to the retarded structure shrinkage by the protection of rigid silica walls of 3DOM-SiO_2[38] during pyrolysis for removal of F127 and carbonization of PF.

Similarly, by using 3DOM-SiO_2 with macropores of 800 nm as the nanoreactor, Fe_2O_3@3DOM-SiO_2 composites with porous iron oxide microspheres of 600 nm in the macropores can be readily fabricated (Figure 7a,b). Through further impregnation with resol/F127/ethanol precursor, 3DOA-Fe_3O_4@*meso*Carbon microspheres with a diameter of 800 nm (denoted as 800 nm-3DOA-Fe_3O_4@*meso*Carbon) were synthesized via the same synthesis strategy and procedure (Figure 7c,d), and the obtained sample has a BET surface area of 326 m^2/g and pore size of 19.0 nm. It is worth noting that the synthesis strategy is applicable for directly coating iron oxide particle with carbon shell in the Fe_2O_3@3DOM-SiO_2 composites via the impregnation procedure similar to that for fabricating 3DOA-Fe_3O_4@*meso*Carbon microspheres, except that no F127 copolymers were used. By using Fe_2O_3@3DOM-SiO_2 composites containing Fe_2O_3 particles of 600 and 800 nm, respectively, 3-D ordered arrays of carbon-coated Fe_3O_4 microspheres with a diameter of 800 and 1200 nm can be fabricated, respectively. The samples were denoted as 800 nm-3DOA-Fe_3O_4@Carbon and 1200 nm-3DOA-Fe_3O_4@Carbon, respectively (Supporting Information, Figure S2). High-

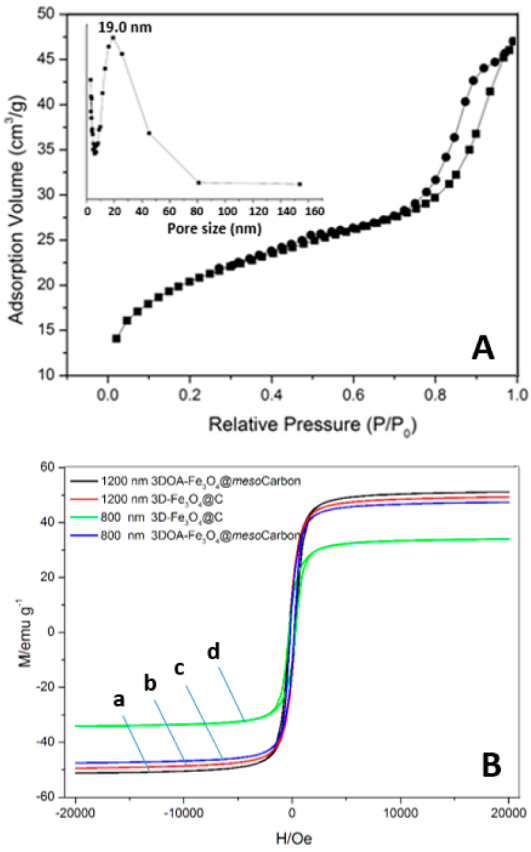

Figure 6. (A) Nitrogen adsorption−desorption isotherms and pore size distribution (inset) of the 1200 nm-3DOA-Fe_3O_4@*meso*Carbon microspheres. (B) Magnetic hysteresis loops of (a) 1200 nm-3D-Fe_3O_4@*meso*Carbon, (b) 1200 nm-3DOA-Fe_3O_4@Carbon, (c) 800 nm-3DOA-Fe_3O_4@*meso*Carbon, and (d) 800 nm-3DOA-Fe_3O_4@Carbon measured at 300 K.

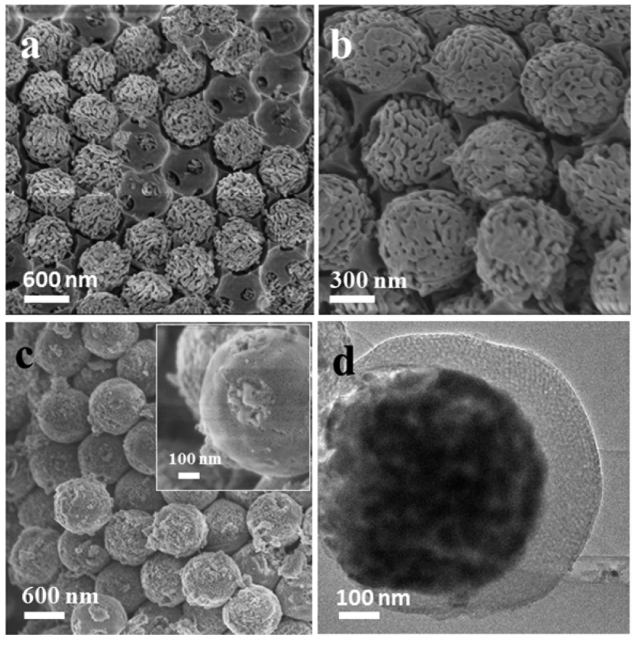

Figure 7. SEM images of (a, b) the Fe_2O_3@3DOM-SiO_2 obtained after replication of the 3-D colloidal crystal of 900 nm PS microspheres. (c) SEM and (d) TEM images of 800 nm 3DOA-Fe_3O_4@*meso*Carbon microspheres.

DOI: 10.1021/am508683p
ACS Appl. Mater. Interfaces 2015, 7, 5312−5319

magnification TEM image clearly indicates the presence of a carbon shell around the iron oxide core (Figure S2, inset).

The magnetic properties of the 3DOA-Fe_3O_4@*meso*Carbon and 3DOA-Fe_3O_4@Carbon microspheres were investigated using a superconducting quantum interference device (SQUID). The magnetic hysteresis loops ($M-H$ loops) of all samples at 300 K are shown in Figure 6B, from which their magnetic properties including saturation magnetization (M_s) and coercivity (H_c) were extracted (Table 1). The M_s values are

Table 1. Saturation Magnetization (M_s) and Coercivity (H_c) for 3DOA-Fe_3O_4@Carbon and 3DOA-Fe_3O_4@*meso*Carbon Microspheres

	saturation magnetization (M_s)	coercivity (H_c)
800 nm-3DOA-Fe_3O_4@Carbon	34	295
800 nm-3DOA-Fe_3O_4@*meso*Carbon	47	182
1200 nm-3DOA-Fe_3O_4@Carbon	50	200
1200 nm-3DOA-Fe_3O_4@*meso*Carbon	52	285

calculated to be 47.0 and 52.0 emu/g for 800 nm- and 1200 nm-3DOA-Fe_3O_4@*meso*Carbon microspheres, respectively. Furthermore, 1200 nm-3DOA-Fe_3O_4@*meso*Carbon microspheres possess larger M_s than 1200 nm-3DOA-Fe_3O_4@Carbon microspheres with the same diameters, which is mainly due to their slightly higher content of magnetic component. Besides, all these iron oxide/C composites possess distinct ferromagnetism as evidenced by the coercivity and the reversible hysteresis behavior at 300 K due to the large crystalline sizes of iron oxides.

To study the microwave absorption properties of the fabricated ordered arrays of magnetite-carbon composites, the reflection loss (RL) values of 3DOA-Fe_3O_4@*meso*Carbon were calculated using the relative complex permittivity and permeability at a given frequency and thickness layer according to the transmit line theory, which are summarized by the two equations below[39,40]

$$\mathrm{RL(dB)} = -20\log_{10}|(Z_{in} - 1)/(Z_{in} + 1)| \quad (1)$$

$$Z_{in} = \sqrt{\mu_r/\varepsilon_r}\tanh[-j(2\pi fd/c)\sqrt{\mu_r/\varepsilon_r}] \quad (2)$$

where ε_r, μ_r, c, f, d, and Z_{in} corresponds to the relative complex permittivity, permeability, velocity of light, microwave frequency in free space, coating thickness, and input impedance of the absorber, respectively. The calculated RL curves for all of the four samples with the thickness of 2 mm in the frequency range of 2−18 GHz were summarized in Figure 8A. (Experimental details for fabricating absorption coating is available in Supporting Information.) The maximum RL values (RL_{max}) of 3DOA-Fe_3O_4@*meso*Carbon samples comprising 1200 nm- and 800 nm-Fe_3O_4@*meso*Carbon are −35 dB at 10 GHz and −37 dB at 11.5 GHz, respectively (Figure 8A,a,b). It suggests these 3DOA-Fe_3O_4@*meso*Carbon microspheres possess comparable RL_{max} values at a coating thickness of 2 mm. By contrast, the RL_{max} values of 1200 nm-3DOA-Fe_3O_4@Carbon and 800 nm- 3DOA-Fe_3O_4@Carbon are −23 dB at 11.2 GHz and −17 dB at 9.5 GHz, respectively (Figure 8Ac,d), both much less than those of the corresponding 1200 nm- and 800 nm-3DOA-Fe_3O_4@*meso*Carbon samples. It suggests that the presence of mesoporous carbon shell can significantly

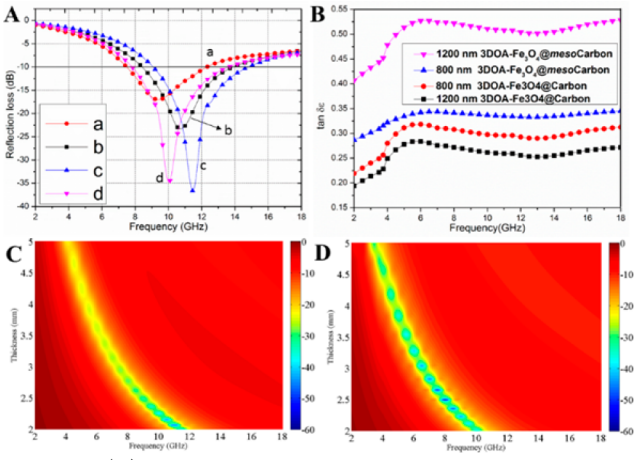

Figure 8. (A) The microwave RL curves of the samples/paraffin composites with a thickness of 2 mm in the frequency range of 2−18 GHz, using (a) 800 nm- and (b)1200 nm-3DOA-Fe_3O_4@Carbon, respectively, and (c) 800 nm- and (d) 1200 nm-3DOA-Fe_3O_4@*meso*Carbon, respectively; (B) the frequency dependence of dielectric loss tangents of the 3DOA-Fe_3O_4@*meso*Carbon and 3DOA-Fe_3O_4@Carbon; (C, D) 3-D representations of RL of 800 nm-3DOA-Fe_3O_4@*meso*Carbon (C) and 1200 nm-3DOA-Fe_3O_4@*meso*Carbon (D).

enhance the performance of microwave absorption of iron oxides. The dielectric loss tangents ($\tan\delta_\varepsilon = \varepsilon''/\varepsilon'$) of all the samples were calculated and summarized in Figure 8B. The values of $\tan\delta_\varepsilon$ for 3DOA-Fe_3O_4@*meso*Carbon samples are larger than 3DOA-Fe_3O_4@Carbon samples in the whole frequency range of 2−18 GHz, implying that the mesoporous carbon shell contributes a stronger dielectric loss. Such a strong dielectric loss of 3DOA-Fe_3O_4@*meso*Carbon microspheres is mainly due to the high surface areas of the ordered mesoporous carbon shells that bring about more defects and dangling-bonded atoms in the pore wall and thus leads to stronger interface polarization compared to carbon shells without mesopores.[41] Moreover, the 3-D representations (Figure 8C,D) of RL values at different coating thicknesses (2−5 mm) for the 800 nm- and 1200 nm-3DOA-Fe_3O_4@*meso*Carbon samples reveal a broader and stronger reflection loss in the whole thickness range, as compared to their counterpart sample of 800 nm- and 1200 nm-3DOA-Fe_3O_4@Carbon samples (Supporting Information, Figure S3). It is worth noting that the RL_{max} value of 1200 nm- 3DOA-Fe_3O_4@*meso*Carbon microspheres can reach −55 dB at a absorption coating thickness of 2.5 mm, which is much larger than those of most carbon-Fe_3O_4 composites reported.[42]

Supporting Information, Figure S4 depicts the complex permittivity real part (ε') and imaginary part (ε'') and the permeability real part (μ') and imaginary part (μ'') of the four samples measured in the frequency range of 2−18 GHz. For 3DOA-Fe_3O_4@*meso*Carbon, ε' and ε'' values are, respectively, less than and higher than those of 3DOA-Fe_3O_4@Carbon microspheres in the whole frequency range. Meanwhile, the frequency dispersion values of μ' and μ'' remain almost constant at 2−18 GHz for the 3DOA-Fe_3O_4@*meso*Carbon and 3DOA-Fe_3O_4@Carbon microspheres, without evident decay even at high frequency band (12−18 GHz). Therefore, it can be concluded that both magnetic loss of Fe_3O_4 and dielectric loss of carbon shell contribute to the absorption dependency on frequency of our samples. In particular, the ordered structure of mesoporous carbon shell and 3-D ordered array of 3DOA-

DOI: 10.1021/am508683p
ACS Appl. Mater. Interfaces 2015, 7, 5312−5319

Fe_3O_4@*meso*Carbon materials bring about a strong reflection and scattering of electromagnetic waves in the mesoporous carbon channels and their core−shell structure.[32,33]

CONCLUSIONS

In summary, for the first time, we report a confined interface coating strategy for the fabrication of novel three dimensionally ordered arrays of core−shell microspheres comprising Fe_3O_4 cores and ordered mesoporous carbon shells, that is, 3DOA-Fe_3O_4@*meso*Carbon, by using 3-D ordered macroporous silica as the nanoreactor for deposition of single iron oxide particle and for further coating iron oxide particle with mesoporous carbon shells. The obtained 3DOA-Fe_3O_4@*meso*Carbon materials have high surface area up to 326 m^2/g and large pore size of ∼19 nm. Because of the combination of the merits of the large magnetic loss of iron oxides, the strong dielectric loss of carbon shell, as well as the strong reflection and scattering of electromagnetic waves of ordered structures of microsphere arrays and mesopore channels, the obtained 3DOA-Fe_3O_4@*meso*Carbon materials exhibit excellent microwave absorption performances with maximum reflection loss of up to −57 dB at 8 GHz and large absorption bandwidth (7.3−13.7 GHz). Because of the versatility of this confined interface coating strategy, it is expected that the design concept can be used for fabrication of a variety of topologically complicated and functionally integrated ordered structures for applications in electronic nanodevices, nanobiosensors, nano-optical systems, etc.

ASSOCIATED CONTENT

Supporting Information

Experimental details for the electromagnetic measurements, SEM images of the colloidal crystal based on uniform PS microspheres of ∼900 nm as building blocks and their templated 800 nm 3D-ordered macroporous SiO_2 (800 nm-3DOM-SiO_2), SEM images of 800 nm-3D-Fe_3O_4@C and 1200 nm-3D-Fe_3O_4@C microspheres. three-dimensional representations of RL of the 800 nm 3D-Fe_3O_4@Carbon and 1200 nm-3DOA-Fe_3O_4@Carbon. This material is available free of charge via the Internet at http://pubs.acs.org.

AUTHOR INFORMATION

Corresponding Authors

*E-mail: yhdeng@fudan.edu.cn. (Y.D.)
*E-mail: rcche@fudan.edu.cn. (R.C.)

Notes

The authors declare no competing financial interest.

ACKNOWLEDGMENTS

This work was supported by the Ministry of Science and Technology of China (973 Project Nos. 2013CB932901 and 2009CB930803), the NSF of China (11274066, 51372041, 51422202, 51172047, 51102050, and U1330118), the specialized research fund for the doctoral program of higher education of China (20120071110007), the innovation program of Shanghai Municipal Education Commission (13ZZ004), Shanghai Rising Star Project of STCSM (12QH1400300), Program for New Century Excellent Talents in University (NCET-12-0123), and the "Shu Guang" Project (13SG02, 09SG01) supported by Shanghai Municipal Education Commission, Shanghai Education Development Foundation, and Shanghai Pujiang Program, and Foundation of State Key Laboratory of Pollution Control and Resource Reuse (Tongji University), China (PCRRF14017).

REFERENCES

(1) Lou, X. W.; Archer, L. A. A General Route to Nonspherical Anatase TiO_2 Hollow Colloids and Magnetic Multifunctional Particles. *Adv. Mater.* **2008**, *20*, 1853−1858.
(2) Weissleder, R.; Moore, A.; Mahmood, U.; Bhorade, R.; Benveniste, H.; Chiocca, E. A.; Basilion, J. P. In Vivo Magnetic Resonance Imaging of Transgene Expression. *Nat. Med.* **2000**, *6*, 351−354.
(3) Zhang, L.; Qiao, S.; Jin, Y.; Yang, H.; Budihartono, S.; Stahr, F.; Yan, Z.; Wang, X.; Hao, Z.; Lu, G. Q. Fabrication and Size-Selective Bioseparation of Magnetic Silica Nanospheres with Highly Ordered Periodic Mesostructure. *Adv. Funct. Mater.* **2008**, *18*, 3203−3213.
(4) Park, J.-H.; Derfus, A. M.; Segal, E.; Vecchio, K. S.; Bhatia, S. N.; Sailor, M. J. Local Heating of Discrete Droplets Using Magnetic Porous Silicon-Based Photonic Crystals. *J. Am. Chem. Soc.* **2006**, *128*, 7938−7946.
(5) Huang, C. C.; Tsai, C. Y.; Sheu, H. S.; Chuang, K. Y.; Su, C. H.; Jeng, U. S.; Cheng, F. Y.; Su, C. H.; Lei, H. Y.; Yeh, C. S. Enhancing Transversal Relaxation for Magnetite Nanoparticles in MR Imaging Using Gd_3^+-Chelated Mesoporous Silica Shells. *ACS Nano* **2011**, *5*, 3905−3916.
(6) Son, S. J.; Reichel, J.; He, B.; Schuchman, M.; Lee, S. B. Magnetic Nanotubes for Magnetic-Field-Assisted Bioseparation, Biointeraction, and Drug Delivery. *J. Am. Chem. Soc.* **2005**, *127*, 7316−7317.
(7) Liu, J.; Qiao, S. Z.; Hu, Q. H.; Lu, G. Q. Magnetic Nanocomposites with Mesoporous Structures: Synthesis and Applications. *Small* **2011**, *7*, 425−443.
(8) Zhang, L.; Qiao, S. Z.; Jin, Y. G.; Chen, Z. G.; Gu, H. C.; Lu, G. Q. Magnetic Hollow Spheres of Periodic Mesoporous Organosilica and Fe_3O_4 Nanocrystals: Fabrication and Structure Control. *Adv. Mater.* **2008**, *20*, 805−808.
(9) Zhu, M.; Wang, C.; Meng, D.; Diao, G. In Situ Synthesis of Silver Nanostructures on Magnetic Fe_3O_4@C Core-Shell Nanocomposites and Their Application in Catalytic Reduction Reactions. *J. Mater. Chem. A* **2013**, *1*, 2118−2125.
(10) Wang, Y. L.; Zhang, L.; Gao, X. H.; Mao, L. Y.; Hu, Y.; Lou, X. W. One-pot Magnetic Field Induced Formation of Fe_3O_4/C Composite Microrods with Enhanced Lithium Storage Capability. *Small* **2014**, *10*, 2815−2819.
(11) Yu, M.; Ling, C.; Liu, M.; Liu, X.; Yuan, K.; Cao, H.; Che, R. Yolk−Shell Fe_3O_4@ZrO_2 Prepared by a Tunable Polymer Surfactant Assisted Sol−Gel Method for High-Temperature Stable Microwave Absorption. *J. Mater. Chem. C* **2014**, *2*, 7275−7283.
(12) Liu, J.; Cheng, J.; Che, R.; Xu, J.; Liu, M.; Liu, Z. Synthesis and Microwave Absorption Properties of Yolk−Shell Microspheres with Magnetic Iron Oxide Cores and Hierarchical Copper Silicate Shells. *ACS Appl. Mater. Interfaces* **2013**, *5*, 2503−2509.
(13) Liu, J.; Che, R.; Chen, H.; Zhang, F.; Xia, F.; Wu, Q.; Wang, M. Microwave Absorption Enhancement of Multifunctional Composite Microspheres with Spinel Fe_3O_4 Cores and Anatase TiO_2 Shells. *Small* **2012**, *8*, 1214−1221.
(14) Sun, G.; Dong, B.; Cao, M.; Wei, B.; Hu, C. Hierarchical Dendrite-Like Magnetic Materials of Fe_3O_4, γ-Fe_2O_3, and Fe with High Performance of Microwave Absorption. *Chem. Mater.* **2011**, *23*, 1587−1593.
(15) Chen, Y.-J.; Xiao, G.; Wang, T.-S.; Ouyang, Q.-Y.; Qi, L.-H.; Ma, Y.; Gao, P.; Zhu, C.-L.; Cao, M.-S.; Jin, H.-B. Porous Fe_3O_4/Carbon Core/Shell Nanorods: Synthesis and Electromagnetic Properties. *J. Phys. Chem. C* **2011**, *115*, 13603−13608.
(16) Guo, H.; Zhan, Y.; Chen, Z.; Meng, F.; Wei, J.; Liu, X. Decoration of Basalt Fibers with Hybrid Fe_3O_4 Microspheres and their Microwave Absorption Application in Bisphthalonitrile Composites. *J. Mater. Chem. A* **2013**, *1*, 2286−2296.
(17) Wang, J.; Xu, J.; Meng, X.; Huang, Y. Template-Assisted Synthesis and Novel Microwave Absorption Properties of Super-

DOI: 10.1021/am508683p
ACS Appl. Mater. Interfaces 2015, 7, 5312−5319

paramagnetic 2D-Nanolamellar Fe_3O_4. *Mater. Res. Bull.* **2014**, *49*, 176−179.
(18) Wang, H.; Dai, Y.; Gong, W.; Geng, D.; Ma, S.; Li, D.; Liu, W.; Zhang, Z. Broadband Microwave Absorption of CoNi@C Nanocapsules Enhanced by Dual Dielectric Relaxation and Multiple Magnetic Resonances. *Appl. Phys. Lett.* **2013**, 102.
(19) He, C.; Qiu, S.; Wang, X.; Liu, J.; Luan, L.; Liu, W.; Itoh, M.; Machida, K.-i. Facile Synthesis of Hollow Porous Cobalt Spheres and Their Enhanced Electromagnetic Properties. *J. Mater. Chem.* **2012**, *22*, 22160−22166.
(20) Yang, H.; Cao, M.; Li, Y.; Shi, H.; Hou, Z.; Fang, X.; Jin, H.; Wang, W.; Yuan, J. Enhanced Dielectric Properties and Excellent Microwave Absorption of SiC Powders Driven with NiO Nanorings. *Adv. Optical. Mater.* **2014**, *2*, 214−219.
(21) Wei, J.; Du, A.; Jin, F.; Wang, Z.; Liu, X. J. The Preparation and High-Frequency Electromagnetic Properties of Ferrimagnetic Bisphthalonitrile-Fe_3O_4 Core-Shell Hollow Microspheres. *J. Magn. Magn. Mater.* **2013**, *340*, 70−75.
(22) Zhu, C.-L.; Zhang, M.-L.; Qiao, Y.-J.; Xiao, G.; Zhang, F.; Chen, Y.-J. Fe_3O_4/TiO_2 Core/Shell Nanotubes: Synthesis and Magnetic and Electromagnetic Wave Absorption Characteristics. *J. Phys. Chem. C* **2010**, *114*, 16229−16235.
(23) Liu, J.; Cheng, J.; Che, R.; Xu, J.; Liu, M.; Liu, Z. Double-Shelled Yolk−Shell Microspheres with Fe_3O_4 Cores and SnO_2 Double Shells as High-Performance Microwave Absorbers. *J. Phys. Chem. C* **2012**, *117*, 489−495.
(24) Wang, Z.; Wu, L.; Zhou, J.; Shen, B.; Jiang, Z. Enhanced Microwave Absorption of Fe_3O_4 Nanocrystals After Heterogeneously Growing with ZnO Nanoshell. *RSC Adv.* **2013**, *3*, 3309−3315.
(25) Yun, J.; Jeon, W.; Drahushuk, L. W.; Baik, S.; Strano, M. S. Extraordinary High Microwave Absorption Cross Section of Ultralong Carbon Nanotubes. *J. Phys. Chem. C* **2014**, *118*, 13757−13763.
(26) Zong, M.; Huang, Y.; Wu, H.; Zhao, Y.; Wang, S.; Zhang, N.; Zhang, W. Facile Synthesis of RGO/Fe_3O_4/Ag Composite with High Microwave Absorption Capacity. *Mater. Lett.* **2013**, *111*, 188−191.
(27) Wang, G.; Gao, Z.; Tang, S.; Chen, C.; Duan, F.; Zhao, S.; Lin, S.; Feng, Y.; Zhou, L.; Qin, Y. Microwave Absorption Properties of Carbon Nanocoils Coated with Highly Controlled Magnetic Materials by Atomic Layer Deposition. *ACS Nano* **2012**, *6*, 11009−11017.
(28) Zhang, K.; Xu, L.-L.; Jiang, J.-G.; Calin, N.; Lam, K.-F.; Zhang, S.-J.; Wu, H.-H.; Wu, G.-D.; Albela, B.; Bonneviot, L.; Wu, P. Facile Large-Scale Synthesis of Monodisperse Mesoporous Silica Nanospheres with Tunable Pore Structure. *J. Am. Chem. Soc.* **2013**, *135*, 2427−2430.
(29) Wu, Z.; Wu, W. D.; Liu, W.; Selomulya, C.; Chen, X. D.; Zhao, D. A General "Surface-Locking" Approach toward Fast Assembly and Processing of Large-Sized, Ordered, Mesoporous Carbon Microspheres. *Angew. Chem., Int. Ed.* **2013**, *52*, 13764−13768.
(30) Zhou, H.; Wang, J.; Zhuang, J.; Liu, Q. A Covalent Route for Efficient Surface Modification of Ordered Mesoporous Carbon as High Performance Microwave Absorbers. *Nanoscale* **2013**, *5*, 12502−12511.
(31) Wang, Y.; Wang, L.; Wu, H. Enhanced Microwave Absorption Properties of α-Fe_2O_3-Filled Ordered Mesoporous Carbon Nanorods. *Materials* **2013**, *6*, 1520−1529.
(32) Guo, X.; Deng, Y.; Gu, D.; Che, R.; Zhao, D. Synthesis and Microwave Absorption of Uniform Hematite Nanoparticles and Their Core-shell Mesoporous Silica Nanocomposites. *J. Mater. Chem.* **2009**, *19*, 6706−6712.
(33) Xu, L.; Tung, L. D.; Spinu, L.; Zakhidov, A. A.; Baughman, R. H.; Wiley, J. B. Synthesis and Magnetic Behavior of Periodic Nickel Sphere Arrays. *Adv. Mater.* **2003**, *15*, 1562−1564.
(34) Meng, Y.; Gu, D.; Zhang, F.; Shi, Y.; Yang, H.; Li, Z.; Yu, C.; Tu, B.; Zhao, D. Ordered Mesoporous Polymers and Homologous Carbon Frameworks: Amphiphilic Surfactant Templating and Direct Transformation. *Angew. Chem., Int. Ed.* **2005**, *44*, 7053−7059.
(35) Deng, Y.; Liu, C.; Liu, J.; Zhang, F.; Yu, T.; Zhang, F.; Gu, D.; Zhao, D. A novel Approach to the Construction of 3-D Ordered Macrostructures with Polyhedral Particles. *J. Mater. Chem.* **2008**, *18*, 408−415.
(36) Ha, S.; Park, O. O.; Im, S. Size Control of Highly Monodisperse Polystyrene Particles by Modified Dispersion Polymerization. *Macromol. Res.* **2010**, *18*, 935−943.
(37) Sun, Z.; Sun, B.; Qiao, M.; Wei, J.; Yue, Q.; Wang, C.; Deng, Y.; Kaliaguine, S.; Zhao, D. A General Chelate-Assisted Co-Assembly to Metallic Nanoparticles-Incorporated Ordered Mesoporous Carbon Catalysts for Fischer−Tropsch Synthesis. *J. Am. Chem. Soc.* **2012**, *134*, 17653−17660.
(38) Wang, M.; Wang, X.; Yue, Q.; Zhang, Y.; Wang, C.; Chen, J.; Cai, H.; Lu, H.; Elzatahry, A. A.; Zhao, D.; Deng, Y. Templated Fabrication of Core−Shell Magnetic Mesoporous Carbon Microspheres in 3-Dimensional Ordered Macroporous Silicas. *Chem. Mater.* **2014**, *26*, 3316−3321.
(39) Che, R. C.; Peng, L. M.; Duan, X. F.; Chen, Q.; Liang, X. L. Microwave Absorption Enhancement and Complex Permittivity and Permeability of Fe Encapsulated within Carbon Nanotubes. *Adv. Mater.* **2004**, *16*, 401−405.
(40) Kumar Srivastava, R.; Narayanan, T. N.; Reena Mary, A. P.; Anantharaman, M. R.; Srivastava, A.; Vajtai, R.; Ajayan, P. M. Ni Filled Flexible Multi-Walled Carbon Nanotube−Polystyrene Composite Films as Efficient Microwave Absorbers. *Appl. Phys. Lett.* **2011**, *99*, 113116.
(41) Wen, B.; Cao, M.; Lu, M.; Cao, W.; Shi, H.; Liu, J.; Wang, X.; Jin, H.; Fang, X.; Wang, W.; Yuan, J. Reduced Graphene Oxides: Light-Weight and High-Efficiency Electromagnetic Interference Shielding at Elevated Temperatures. *Adv. Mater.* **2014**, *26*, 3484−3489.
(42) Du, Y.; Liu, W.; Qiang, R.; Wang, Y.; Han, X.; Ma, J.; Xu, P. Shell Thickness-Dependent Microwave Absorption of Core−Shell Fe_3O_4@C Composites. *ACS Appl. Mater. Interfaces.* **2014**, *6*, 12997−13006.

DOI: 10.1021/am508683p
ACS Appl. Mater. Interfaces 2015, 7, 5312−5319